Vertical orbital structure around the Lagrangian points in barred galaxies

Link with the secular evolution of galaxies

Mercè Ollé[1,2] **and Daniel Pfenniger**[1]

[1] Geneva Observatory, CH-1290 Sauverny, Switzerland
[2] ETSEIB, Dept. Matemàtica Aplica I, Diagonal 647, 08028 Barcelona, Spain

Received dd Month, yyyy/ Accepted dd Month, yyyy

Abstract. The stability of the Lagrangian points and the vertical periodic orbits around them is examined in the context of barred galaxies. A transition from stability to complex instability appears for the points L_4 and L_5 when the strength of the bar is sufficiently large. The Hopf-like bifurcation associated to such a transition is *inverse* and its effects on the central family of periodic orbits and neighbouring orbits are described. This instability can play an important role for barred galaxies secularly increasing the strength of their bar, because a sudden full destabilization of matter around these Lagrangian points must occur. This effect is demonstrated with a sample of trajectories diffusing away from the corotation circle several 10 kpc radially, and several kpc out the galaxy plane.

Key words: barred galaxies – galaxy evolution – periodic orbits – complex instability

1. Introduction

In contrast with elliptical galaxies, which rotate slowly, barred galaxies must possess several stationary points in their stellar part, the Lagrangian points, because their bar rotate rapidly, as generally admitted. In addition to the potential minimum at the galaxy centre, these galaxies have four additional stationary points in the rotating frame of the stellar bar, along the major and minor axes in the galaxy plane (see e.g., Binney & Tremaine 1987, p. 137). The corotation region therefore plays a fundamental role in the dynamics in barred galaxies (and other rotating patterns).

The most important topological constraint in a barred galaxy is given by the zero velocity surface of the only global integral of the system, the Jacobi integral H (the Hamiltonian expressed in coordinates co-rotating with the bar). If the value of this integral is lower than the value necessary to co-rotate with the Lagrangian point near the end of the bar, motion is confined either inside a lenticular shape, or outside a one-sheet hyperboloidal surface beyond the corotation radius (Fig. 1, top). For increasing values of H, the lenticular and hyperboloidal surfaces meet and merge, which opens a hole around $L_{1,2}$ allowing to cross corotation and eventually to escape (Fig. 1, middle). This hole widens to the whole corotation circle at still higher values (Fig. 1, bottom). At any value of this integral there always exists a forbidden region above the bar that slowly recesses as H increases.

To gain further understanding on the bar dynamics, one can adopt the famous Poincaré general strategy for conquering non-integrable systems: one should first characterize the stability of the fixed points, then explore the properties of the periodic orbits associated with the fixed points. In turn, the stability properties of the periodic orbits give insight on their neighbourhood: stable periodic orbits are mostly surrounded by quasi-periodic orbits, while unstable periodic orbits by chaotic orbits. In principle, the process can extend to higher order periodic orbits; in practice the complexity of the high-order orbits in non-integrable systems rapidly confuses the situation.

Our experience has been that the knowledge of the main families of periodic orbits, gained by the work of many people, is invaluable not only to understand real barred galaxies, but also to develop insight. For example one can immediately picture out what is happening in complex situations developing in N-body simulations of barred galaxies (e.g., Pfenniger & Friedli 1991).

The stable periodic orbits trapping effectively stars are particularly important to understand the structure of these galaxies and the motion of its stars, but the unpopulated periodic orbits are important too for predicting the fate of small mass perturbations, such as infalling dwarf galaxies or gas clouds.

Historically, the order of study of barred galaxies has not followed exactly the Poincaré plan. Because the properties of the central fixed point are trivial in the principal plane, people have immediately concentrated the ef-

Send offprint requests to: Daniel.Pfenniger@obs.unige.ch

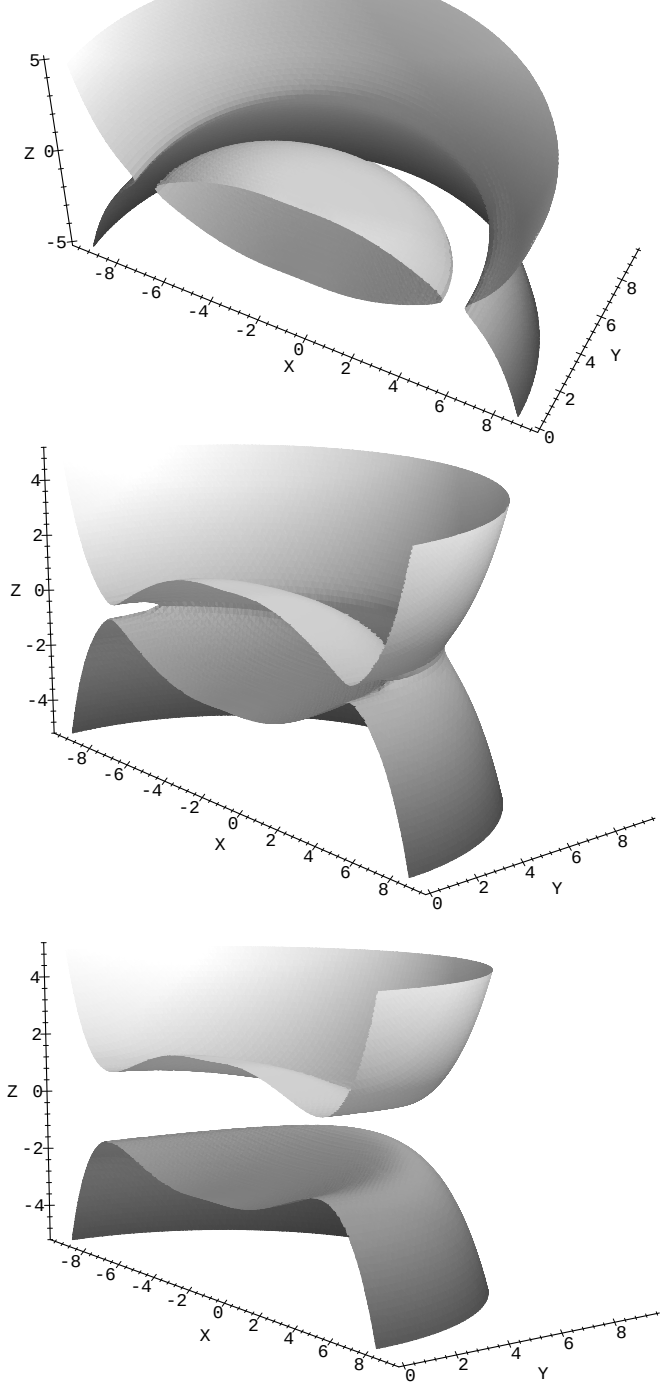

Fig. 1. Topology constraint to motion existing in a barred galaxy due to the Jacobi integral H, shown in the half-space $y > 0$. The bar major axis is aligned with the x-axis, and the rotation axis is the z axis. The shaded surface shows the zero-velocity surface beyond which no motion does exist for three particular values h of the Hamiltonian H.
Top: At low h, particles are confined either inside a lenticular shape in the bar region, or outside a surface similar to a one-sheet hyperboloid. **Middle:** At higher h the two surfaces join at the corotation locus allowing orbits to crossing it. **Bottom:** At still higher h forbidden regions above the galactic poles persist for bound particles.

associated with the circular orbits in the vanishing-bar limit, first in the galaxy plane, and then in 3D. Only later did we look at the radial orbits along the rotation axis, so associated with the central point (Martinet & Pfenniger 1987; Pfenniger 1987, hereafter MP87 and P87). In systems with 3 degrees of freedom we have the phenomenon of *complex instability* which is not possible in systems with 2 degrees of freedom. This kind of instability appears, for example, in the Elliptic Restricted Three-Body Problem (Broucke 1969), in the problem of planetary systems (Hadjidemetriou 1975), or in galactic dynamics (Magnenat 1982; Contopoulos & Magnenat 1985; Martinet & Pfenniger 1987; Pfenniger 1985b, 1990; see also Pfenniger 1995 for a short review).

On the other hand the properties of the Lagrangian points remained for many years insufficiently understood, although the orbits in the plane developing around them were investigated (Contopoulos 1981, 1988; Contopoulos & Grosbøl 1989), exhibiting an intimidating wealth of structures. The precise conditions of stability of these points being not clear, we investigated its properties some years later (Pfenniger 1990, hereafter P90). It turned out that in the typical situations of barred galaxies, these points are either always unstable (around the Lagrangian points L_1 and L_2 at the ends of the bar major axis[1]), or not far from being marginally *complex unstable* around the Lagrangian points L_4 and L_5 along the minor axis in the self-consistent models issued from N-body simulations. A marginal state of fixed points means that profound changes of the phase space structure around these points can be expected for a small change of the bar parameters.

So today there remains still an unexplored major region of phase space of barred galaxies: the vertical orbit structure developing from the Lagrangian points. This is the purpose of this study to sketch their main properties.

In Section 2, we consider a barred galaxy model made of a $n = 2$ Ferrers bar embedded in a Miyamoto-Nagai disk, with a variable bar parameter. In Section 3, the derivation of the equilibrium points and the stability diagram are briefly recalled. In Section 4, we describe how the transition from stability to complex instability appears for the Lagrangian points $L_{4,5}$ when the bar strength is increased. The propagation of this transition on the family of periodic orbits around these points is also given, and we determine the orientation of the bifurcation at the transition. In Section 5, the Lagrangian points $L_{1,2}$ are considered. They are always simply unstable. The periodic orbits around them and their bifurcations are numerically

[1] There is no general agreement in the literature about the names of the Lagrangian points, except that the first three points are co-linear with the bar, or the massive bodies in the restricted three-body problem. Here L_1 and L_2 are symmetrically aligned with the bar along the x-axis, L_3 is at the centre, and L_4 and L_5 are symmetrically aligned perpendicularly to the bar along the y-axis, in the galaxy plane.

these orbits are not useful for understanding the galactic structure. In Section 6, we discuss briefly the horizontal and vertical stability of the long and short periodic orbits circling around $L_{4,5}$. Finally, in Section 7, we consider the non-linear effect of instability on sample orbits and their diffusion across the galaxi, and discuss in Section 8 some implications of the found results for galaxy secular evolution.

2. Barred galaxy potential

For the sake of comparison, the barred galaxy potential used here is the one described in Pfenniger 1984 (P84). As often verified, the precise density shape far from the considered orbits is not important when describing the major orbits of a galactic potential: indeed their shapes depend mostly on the main *symmetries* of the problem.

The potential derives from two mass components, a Miyamoto-Nagai (1975) disc, whose potential reads,

$$\Phi_{\rm D}(x) = -\frac{GM_{\rm D}}{\sqrt{x^2+y^2+\left(A+\sqrt{B^2+z^2}\right)^2}} \qquad (1)$$

and a triaxial $n=2$ Ferrers (1877) bar of semi-axes a, b, c, whose density $\rho(x)$ is expressed by

$$\begin{aligned} \rho(x) &= \tfrac{105 M_{\rm B}}{32\pi abc}(1-m^2)^2 \quad \text{for } m \le 1 \\ &= 0 \qquad\qquad\qquad\quad \text{for } m > 1 \ , \end{aligned} \qquad (2)$$

where m is the scaled "ellipsoidal radius":

$$m^2 = \frac{x^2}{a^2}+\frac{y^2}{b^2}+\frac{z^2}{c^2}\,, \qquad a>b>c>0\,. \qquad (3)$$

The corresponding potential $\Phi_{\rm B}$ and forces are given in a closed form suited for numerical treatment in P84[2][3]. Here we adopt the now widespread convention of aligning the bar major axis with the x-axis. The corotation radius $R_{\rm cr}$ is put at the end of the major semi-axis a of the bar. The values of the fixed parameters are $A=3$, $B=1$, $a=6$, $b=3$, and $c=2.5$, while $GM_{\rm D}$ and $GM_{\rm B}$ are variable satisfying $G(M_{\rm D}+M_{\rm B})=1$.

The main change with the "main model" in P84 is the adoption of a much thicker, nearly prolate bar ($a/c=2.4$ instead of 10), less eccentric ($a/b=2$ instead of 4), but more massive ($GM_{\rm B}\approx 0.6$ instead of 0.1), so that the bar strength remains similar.

The first reason to adopt a nearly prolate bar is that the belief in the 80's that bars should be very flat in z Hamabe 1984) which was based on a single case, NGC 4762, has not resisted the subsequent evidences coming from N-body simulations and from the shape of the Milky Way Bar (e.g., Zhao 1996; Fux 1997). While it is possible that flat growing bars start from a thin disk, the resulting fierce vertical resonances induced by the bar necessarily bend and inflate it, as shown clearly in the N-body simulations of Raha et al. (1991) and ours. As consequence a thick prolate bar demands a smaller ratio a/b and a larger bar mass in order to yield, when combined with the Miyamoto-Nagai disk, face-on projected isophotes compatible with the ones of barred galaxies (and N-body bars) with axis-ratios of the order of 2/1.

The second reason to choose a more massive but less eccentric bar is that the stability properties of the Lagrangian points $L_{4,5}$ are then compatible to those found in N-body simulations, i.e. in self-consistent mass models (P90).

The prime goal to reach with this potential, i.e. to get a relatively realistic mass model computable with precision but without excessive compromise linked with easily tractable analytical formulae, is then achieved.

The length unit can be conveniently taken as the kpc, the time unit as 1 Myr, and the mass unit of the order of $2\cdot 10^{11}\,{\rm M}_\odot$.

3. Equilibrium and stability diagram

The equations of motion used are those defined by the Hamiltonian H, in a frame of reference rotating about the z-axis with the frequency Ω, and the x-axis aligned with the long axis of the bar, that is,

$$\dot{Q} = \frac{\partial H}{\partial P}, \qquad \dot{P} = -\frac{\partial H}{\partial Q}, \qquad (4)$$

where $Q=(x,y,z)$, $P=(p_x,p_y,p_z)$ are the canonical variables and the expression of H is

$$H = \frac{1}{2}(p_x^2+p_y^2+p_z^2) + \Phi(x,y,z) - \Omega\,(xp_y - yp_x), \qquad (5)$$

with $\Phi(x,y,z)=\Phi_{\rm D}+\Phi_{\rm B}$ the potential described in Section 2. Since Φ is symmetric in z, it follows that $\Phi_z(x,y,0)=0$ and the equilibrium points lie in the plane $z=0$. More specifically, the Lagrangian points $L_{1,2}$ on the x axis are obtained from the equation $\Phi_x(x,0,0)-\Omega^2 x = 0$, and the Lagrangian points $L_{4,5}$ on the y-axis from $\Phi_y(0,y,0)-\Omega^2 y = 0$.

Linearizing the equations of motion at $z=0$ and around a stationary point, we obtain the variational equations,

$$\begin{aligned} \dot{\delta x} &= \delta p_x + \Omega\,\delta y, & \dot{\delta p_x} &= -\Phi_{xx}\,\delta x - \Phi_{xy}\,\delta y + \Omega\,\delta p_y, \\ \dot{\delta y} &= \delta p_y - \Omega\,\delta x, & \dot{\delta p_y} &= -\Phi_{xy}\,\delta x - \Phi_{yy}\,\delta y - \Omega\,\delta p_x, \\ \dot{\delta z} &= \delta p_z, & \dot{\delta p_z} &= -\Phi_{zz}\,\delta z, \end{aligned} \qquad (6)$$

where the δ's denote the linear variations and the potential second derivatives Φ_{xx}, Φ_{xy}, Φ_{yy}, and Φ_{zz} are constants

[2] The Fortran routines are freely available on request to DP.

[3] We take the opportunity to correct here misprints in the Appendix of P84: First, the second term of W_{010} in (A17) should read $-2F(\phi,k)/(a^2-b^2)\sqrt{a^2-c^2}$. Anyway, the shorter expression (A19) is used in calculations of W_{010}. Second, the terms W_{210}, W_{021}, and W_{102} in (A20) should have opposite signs, as verified by using (A11). These misprints have no consequences on the results in P84, since the correct formulae are used in the Fortran routines.

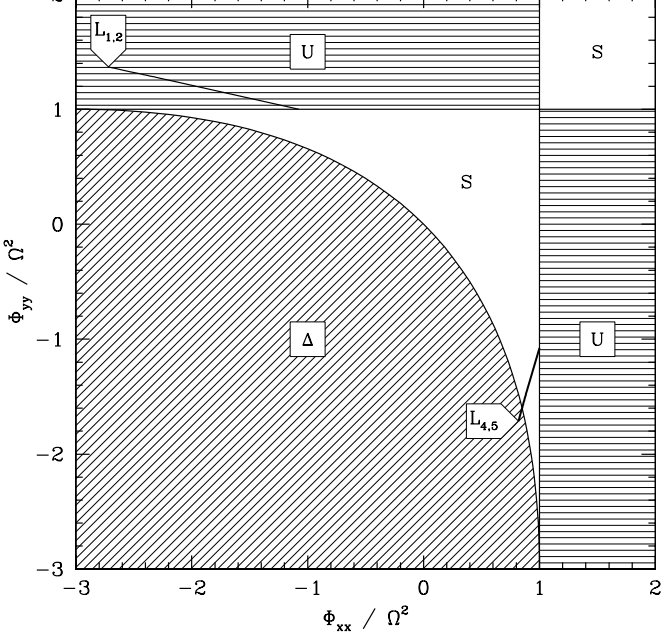

Fig. 2. Stability diagram which delineates the stable and unstable regions of the plane $(\Phi_{xx}/\Omega^2, \Phi_{yy}/\Omega^2)$. S stands for stable, U simple unstable, and Δ complex unstable (notation as in Contopoulos & Magnenat 1985). The position of the Lagrangian points is indicated when the bar mass $GM_{\rm B}$ varies from 0 (on the S–U marginal line) to 0.8 (at the tip of the mark).

evaluated at the stationary point. The terms Φ_{xz}, Φ_{yz} do not appear in Eq. (6) since Φ_z vanishes at $z = 0$.

It is clear from Eq. (6) that the pair of equations for δz, δp_z separates from the rest and corresponds to an independent bounded harmonic motion if $\Phi_{zz} > 0$. In sufficiently thin disks $\Phi_{zz} > 0$ is equivalent to requiring the positivity of mass at $z = 0$ by Poisson's equation. *Therefore we conclude that at each Lagrangian point a family of periodic orbits must start and continue transversally to the galaxy plane.* Contrary to the axial orbits passing through the centre L_3, these transverse orbits will not remain straight at non-infinitesimal amplitudes and their shape will be less obvious to determine.

Before computing these orbits it is useful to calculate their stability at low amplitude, which is just the stability of the relevant Lagrangian point. As determined in P90, one has to calculate the second derivatives of the potential Φ_{xx}, Φ_{yy} for a given pattern speed Ω to find whether the motion around them is characterized by stability or any other type of instability.

In Fig. 2 we plot the position of the Lagrangian points in the relevant stability diagram discussed in P90 (see Fig. [1], p. 57). When $GM_{\rm B}$ increases from 0 to 0.8, the points $L_{1,2}$ remain simply unstable, moving toward the upper left of the Figure; but the points $L_{4,5}$ see a transition from stability to complex instability (at $G\tilde{M}_{\rm B} =$ This is a crucial property of strong bars found in N-body simulations (P90).

4. Vertical motion around $L_{4,5}$

Our aim in this section is to describe the effect of the transition stability-complex instability on the family of 3-dimensional periodic orbits starting at the Lagrangian points $L_{4,5}$.

4.1. Families of 3-D periodic orbits

With standard Newton-type techniques improved by a least-squares approach to treat numerical degeneracies (see e.g., P84, P85b) the vertical periodic orbits starting at the Lagrangian points $L_{4,5}$ and their type of stability/instability are calculated. Owing to the symmetry of the problem only the L_4 orbits need to be discussed.

In a first approach we carry out a numerical exploration of the family of 3-D periodic orbits for different values of $GM_{\rm B}$ close to the transition, more specifically, $GM_{\rm B} = 0.55, 0.60, 0.621, 0.622$, keeping $GM_{\rm B}+GM_{\rm D} = 1$. For any value of $GM_{\rm B}$ fixed, we obtain the corresponding family of periodic orbits, beginning at $L_{4,5}$ with $p_z = 0$, continuing with increasing p_z up to a maximum value, and decreasing down to $p_z = 0$, where the family ends on the nearly circular retrograde family in the galaxy plane, at a 2-periodic (period doubling) bifurcation. Fig. 3, top, illustrates the evolution of shape of the orbits along the family. Near $L_{4,5}$ the orbits look like twisted and bended eights, the extremities being bent toward the galaxy centre. At higher amplitudes and higher h the two eight lobes lean more and more toward the plane until they merge with the retrograde family at a period doubling bifurcation.

Following Broucke (1969), the linear stability of a 3D periodic orbit is given by 3 real parameters, equivalent but more economic to discuss than the 4 complex eigenvalues that would characterize the linear stability of a periodic orbit in an autonomous 3D Hamiltonian system. The *stability parameters* b_1, b_2 and Δ are explained in detail in, e.g., P85a. We just recall that a periodic orbit is stable whenever the two b_i are real and in the interval $(-2, 2)$. If Δ is real and negative, the b_i must be complex and we have complex instability.

Figure 4 shows the evolution of the stability parameters b_1, b_2 as the amplitude varies for different bar masses. We see that there are different critical orbits announcing resonances: five with $b_1 = -2$ (the last one is the terminating orbit of the family) and one (two for $GM_{\rm B} = 0.6$) with $b_1 = 2$; those orbits are candidates to possible bifurcations of other families, which we have not followed, our aim being to give a first order description of the 3D dynamics.

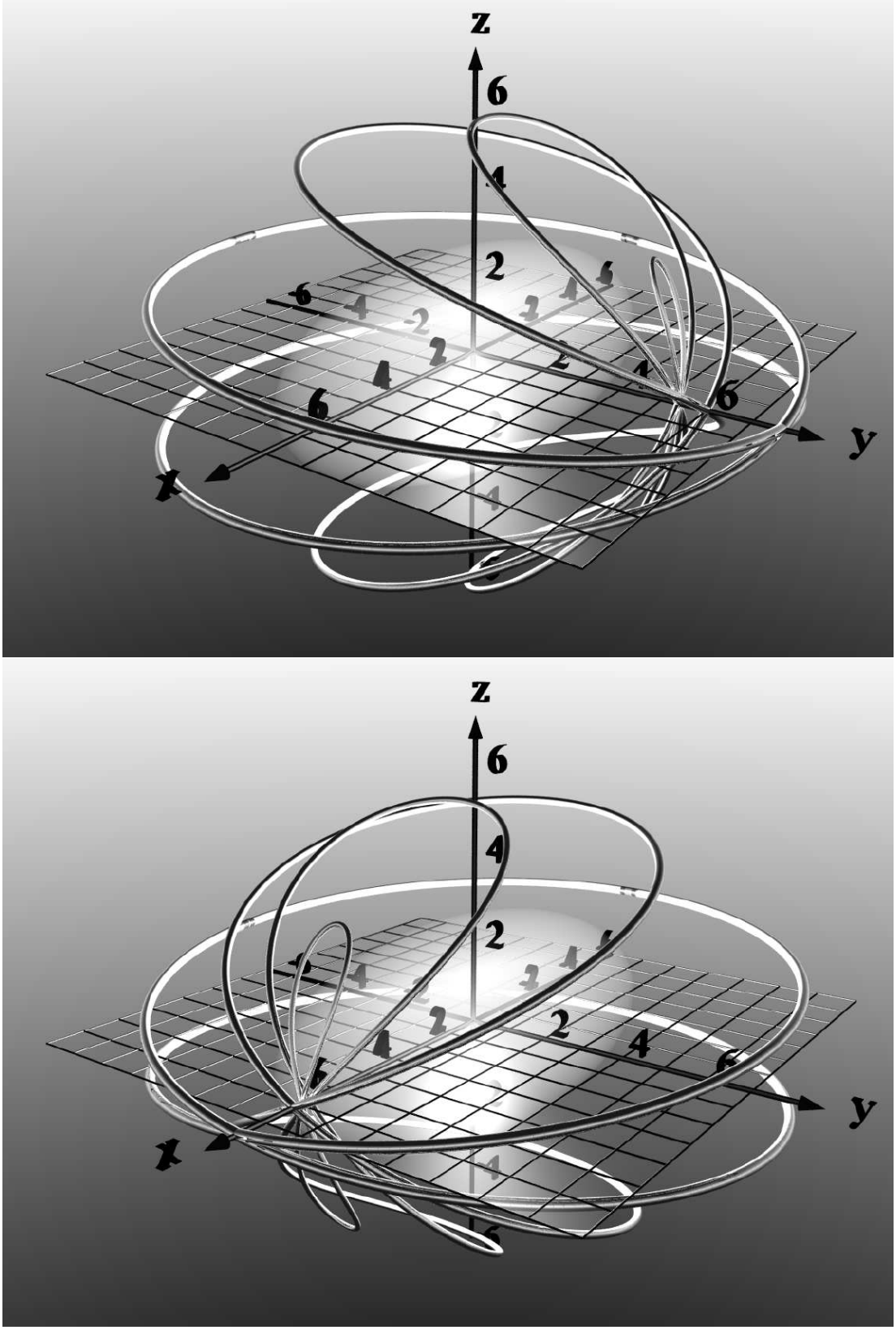

Fig. 3. Some members of the family of 3-D periodic orbits starting at $L_{4,5}$ (top) and $L_{1,2}$ (bottom) and ending on the nearly circular retrograde family in the galaxy plane at a period-doubling bifurcation. The tube thickness increases proportional to the Hamiltonian value h. The semi-transparent ellipsoid corresponds to the model Ferrer's bar

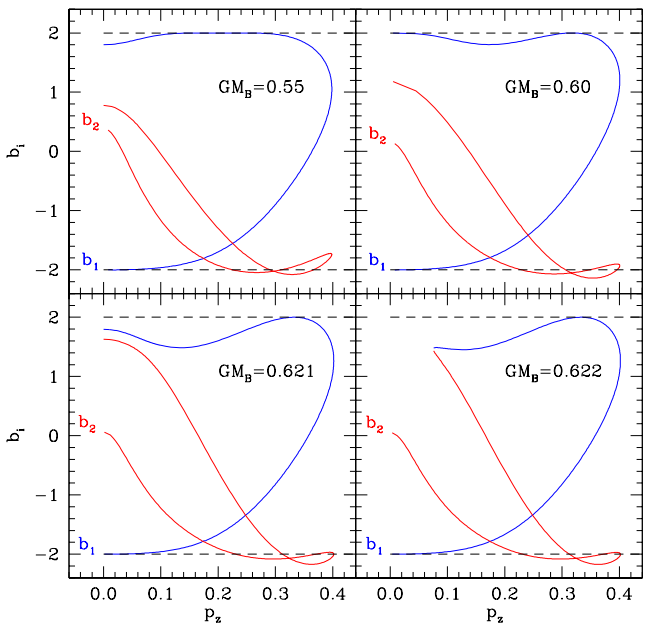

Fig. 4. Stability parameters of the family of 3-D periodic orbits around $L_{4,5}$ for $GM_{\rm B} = 0.55$, 0.60, 0.621, and 0.622. In the frame $GM_{\rm B} = 0.55$ the curve b_1 gets very close to the value 2, but is not strictly tangent over a finite interval as one might suppose from the plot.

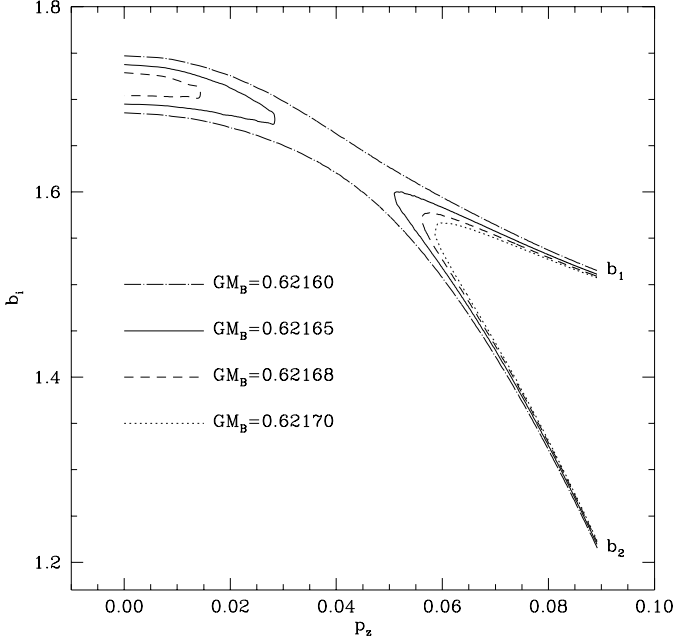

Fig. 5. Stability parameters of the family of 3-D periodic orbits around $L_{4,5}$ for $GM_{\rm B} = 0.62160$, 0.62165, 0.62168, and 0.62170.

Then, for a fixed $GM_{\rm B}$ we focus our attention on the evolution of the stability at the beginning of the family, when p_z varies in the interval $[0., 0.1]$ (which would correspond to speeds transverse to the plane up to approximately 100 km/s).

From Fig. 4 we see that for the values of $GM_{\rm B} = 0.55$ 0.60, and 0.621, that is $GM_{\rm B} < G\tilde{M}_{\rm B}$, the periodic orbits are always stable, while for $GM_{\rm B} = 0.622 > G\tilde{M}_{\rm B}$, they are complex unstable (the complex b_1 and b_2 are not plotted in the Figure) for a certain interval and become stable afterwards, that is, when decreasing p_z, there is a minimum value of p_z for which the curves b_1 and b_2 coincide and become complex for smaller p_z.

Now, we analyze the precise evolution through the marginal value, for $GM_{\rm B}$ increasing from 0.621 to 0.622. We show in Fig. 5, that *already before* achieving the marginal value, there is an interval of stable periodic orbits at low amplitude, an interval of complex unstable ones at an intermediate amplitude, and an interval of stable ones at high amplitudes (for instance Fig. 5, when $GM_{\rm B} = 0.62165$).

So, we can conclude that the effect of the change of stability (S-Δ) for the Lagrangian points $L_{4,5}$ on the stability character of the periodic orbits around them is to delay the transition, and for increasing $GM_{\rm B}$ the stability of the periodic orbits is given by the following patterns: *stable, stable–complex unstable–stable, complex unstable–stable*. In a schematic way, the propagation of the transition is shown by the *transition diagram* given in Fig. 6. It is visible that the concerned mass interval is tiny: 0.001. Above the critical mass value $G\tilde{M}_{\rm B}$ all the periodic orbits with transverse velocities less than $\sim 0.06 \approx 60\,$km/s are complex unstable.

4.2. Orientation of the bifurcation

Once we have obtained the transition diagram, we focus our attention on the effect of the bifurcation on the central periodic family. On one hand, as far as the *bifurcating manifolds* from the transition orbit are concerned, we know that, if k denotes the rotation number of the transition orbit, there bifurcate periodic orbits or 2D invariant tori depending on whether k is rational or irrational respectively (see P85a; Heggie 1985).

The transition to complex instability is the Hamiltonian version of the Hopf bifurcation in dissipative systems. Considering the *orientation* of the bifurcation, the bifurcating structures may be "direct" (they unfold on the unstable side), or "inverse" (they unfold on the stable side). According to the orientation, the effect on the complex unstable central orbit is completely different: in the direct case it confines the chaotic orbits for some time, which may be long, or, in the inverse case, it allows an immediate escape (see P85ab for details).

Now the orientation of the bifurcation for the family of periodic orbits around $L_{4,5}$ given in the diagram above is considered. We examine both the "vertical" evolution

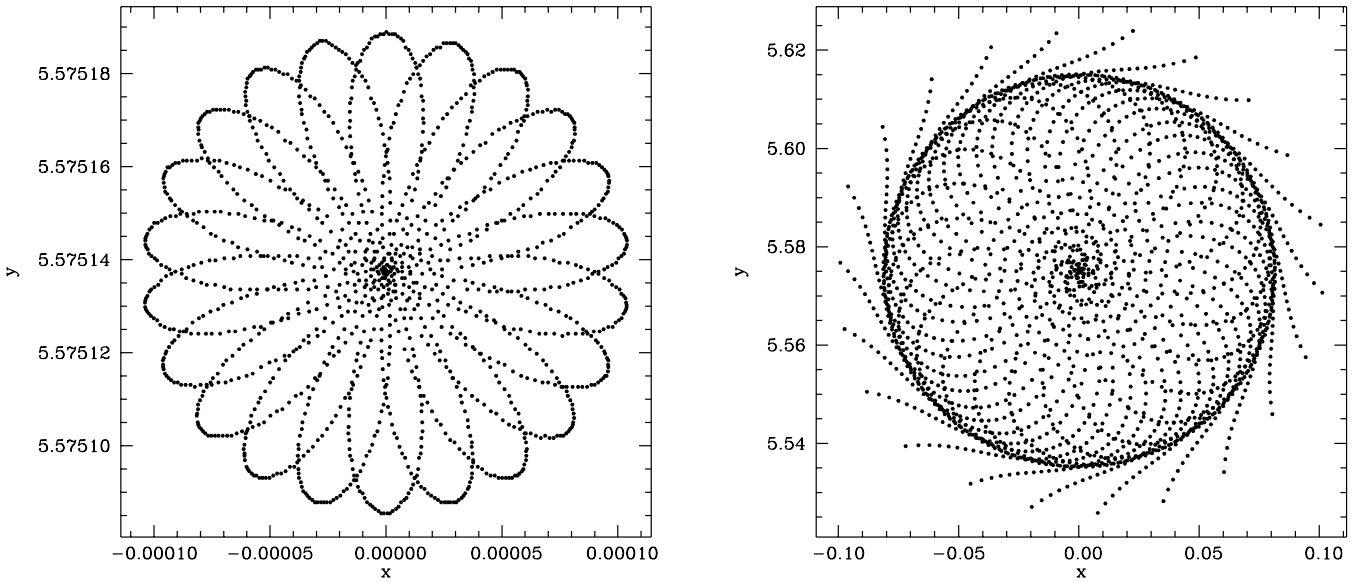

Fig. 7. a: (x, y) projections of the consequents of an orbit in the Poincaré section $z = 0$, $p_z > 0$ belonging to the stable region. **b:** Envelope of the stable invariant tori around the central family obtained with the anti-dissipative method ($D = 1.00001$). The same initial conditions are taken in both cases: $x = z = p_y = 0$, $y = 5.5751369$, $p_x = -0.36897282$, $p_z = 0.027568287$.

Fig. 6. Transition from stability to complex instability in a diagram $GM_{\rm B} - p_z$. The complex unstable regime is marked by Δ, the stable one by S.

with variable p_z and $GM_{\rm D}$ fixed, and the "horizontal" one with variable $GM_{\rm B}$ and p_z fixed. The same procedure follows in the two cases. Let us fix for instance, $GM_{\rm B} = 0.62165$; from the bifurcation diagram, when varying p_z we have two transitions from stability to complex instability, corresponding to $p_z = p_{z1}$ and $p_z = p_{z2}$ (see Fig. 5). To determine whether the associated bifurcations are direct or inverse, we take initial conditions close to the ones of a complex unstable periodic orbit with $p_z > p_{z1}$ and p_z close to p_{z1} (the same happens for a complex unstable orbit with p_z close to p_{z2} and $p_z < p_{z2}$). If we plot the consequents of the corresponding orbit on the Poincaré section $z = 0$, they are not confined at all and the orbit escapes. Thus, the bifurcation unfolds on the stable side, i.e., it is of *inverse type*.

It is interesting to see this effect on the invariant tori surrounding the stable central family. In order to reach the last invariant torus, we use the anti-dissipative procedure described in P85ab for symplectic mappings and galactic potentials. It consists in perturbing the equations of motion by an anti-dissipative term (i.e., by dilating phase-space volumes with time) proportional to a factor D slightly larger than 1 but conserving the initial Hamiltonian value h. We take initial conditions of an orbit belonging to the stable region; for $D = 1$, the Hamiltonian case, the orbit lies on a torus (see Fig. 7a). For $D = 1.00001$, the consequents on the section $z = 0$ explore larger and larger tori at constant h until they reach the last one. Then there is a sudden escape as visible on the last outer points in

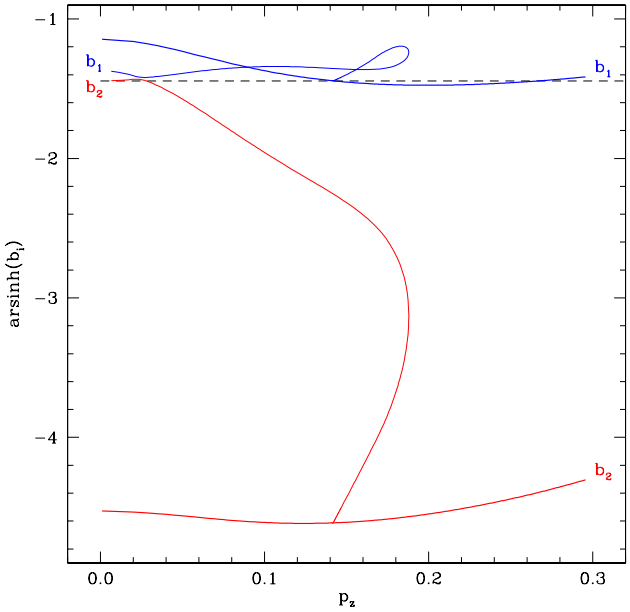

Fig. 8. Low-h part of the stability parameters b_1 and b_2 of the orbit family starting from $L_{1,2}$ (thick curves) as a function of $\dot{z} = p_z$, and a bifurcating family (thin curves) in the range $0 \leq p_z \leq 0.3$. Stable orbits are those which have b_1 and b_2 above the dotted line, which corresponds to $b_i = -2$ (or, $\mathrm{arsinh}(b_i) = -1.443\ldots$).

Fig. 7b. An upper bound of the extent of the invariant tori is provided by the envelope of the accumulated points just before the escape. Fig. 7 thus confirms that the Hopf-like bifurcation unfolds on the stable side of the varying parameter $GM_{\rm B}$, i.e., it is of inverse type.

5. Vertical motion around L_1 and L_2

For the sake of completeness, we now consider the vertical motion around the Lagrangian points $L_{1,2}$ located on the x-axis at some distance from the bar ends. (The vertical motion close to the equilibrium point $L_3 = (0,0,0)$, so along the rotational z-axis, was described in MP87 and P87.)

As we see from Fig. 2, the points $L_{1,2}$ remain simply unstable when varying $GM_{\rm B}$ from 0 to 0.8, there is no change of instability type once the bar strength is non-zero. Contrary to $L_{4,5}$, there is no transition S-Δ. Thus, no qualitative change in the phase space structure is expected around the orbits starting at $L_{1,2}$ over the whole range of reasonable bar strengths.

The search of 3-dimensional periodic orbits around the equilibrium points proceeds as for $L_{4,5}$, though owing to the strong simple instability of $L_{1,2}$ more care must be adopted in choosing the initial trial conditions. Otherwise, the Newton algorithm would rarely converge toward the uation method, we obtain two families of periodic orbits, symmetric with respect to the $z = 0$ plane, with initial conditions $(x, 0, 0, 0, p_y, p_z)$ and $(x, 0, 0, 0, p_y, -p_z)$. Some members of this family are shown in Fig. 3. The morphology of the whole family is little dependent on the bar strength. As for the orbits starting at $L_{4,5}$, at low amplitudes these orbits also start as a twisted and bended 8-shape crossing the galactic plane. They extend around the whole bar as h increases, until joining the retrograde orbit family in the plane, often called x_4 (R in P84)[4], and outside the corotation radius at a period-doubling bifurcation of the latter.

For the bar and disk parameters fixed as usual, we choose $M_{\rm B} = \tilde{M}_{\rm B}$, the marginal stability value for $L_{4,5}$. Then $|x(L_{1,2})| = 6.27094695$. The low-$h$ evolution of their stability parameters b_i when increasing h is shown in Fig. 8. As for the families starting at $L_{4,5}$, at high h the b_i-curves turn back to 0 in p_z when the families converge toward the retrograde main family in the galaxy plane.

A natural question that arises is whether there exist *stable* periodic orbits bifurcating from the unstable family associated to $L_{1,2}$. The answer is positive. At first, unstable bifurcating orbits begin at a critical orbit with $p_z \sim 0.14$, increase up to a maximum value and decrease down to zero, i.e. they end with being planar retrograde orbits, for which $b_2 = -2$ (see Fig. 8). In between, critical orbits with $b_2 = -2$ exist, as just visible in Fig. 8. Thus an interval with *stable* orbits does exist. Of course, from the critical points new periodic families must start. However, all these orbits are too far from the Lagrangian points to be relevant here, so we do not describe them any longer.

6. Lagrangian orbits in the plane

An other question that could be raised is whether the vertical and radial instability found around $L_{4,5}$ as the bar strength increases, has some correspondence in the long and short period orbits circulating around the Lagrangian points in the galaxy plane, the Lagrangian periodic orbits. These orbits and their stability in the plane have been investigated particularly by Contopoulos (1988), who finds an amazing wealth of structures, such as spiral characteristics. In P84, where $L_{4,5}$ were stable, we investigated briefly the vertical stability of these orbits without finding any significant vertical instability.

Here we calculate the radial and vertical stability of the long and short period Lagrangian orbits for the parameters of the barred galaxy model, varying $GM_{\rm B}$. We describe only briefly the general trends, without entering

[4] The terminology x_1, x_2, x_3 and x_4 was introduced by Contopoulos & Papayannopoulos (1980). A student friendly and mnemonic terminology was proposed by Athanassoula et al. (1983): B (for bar sustaining orbits), A, A' for anti-bar orbits) and R (for retrograde orbits).

become rapidly unwidely, without bringing better insight to the paper topic.

When $M_{\rm B}$ is small ($\ll \tilde{M_{\rm B}}$), these orbits are far from being vertically unstable. As the bar strength increases, they become more and more radially unstable over an increasing portion of their characteristic. Vertical instability does occur in a significant way as $M_{\rm B}$ approaches $\tilde{M_{\rm B}}$, but for orbits which are already much more unstable radially. The level of vertical instability is always significantly lower than the radial instability.

Thus we conclude that the Lagrangian orbits reflect and slightly anticipate the general instability at $L_{4,5}$. This could be expected when knowing that $L_{4,5}$ undergoes an inverse Hopf-like bifurcation, because then the volume of stable invariant tori around the stable point shrinks (down to zero) *before* reaching the transition to complex instability.

7. Diffusion from the corotation radius

After having described the instabilities affecting the main periodic orbits around the Lagrangian points, a natural question is to characterize the neighbouring phase space: how fast and how far in R and $|z|$ are the neighbouring chaotic orbits diffusing from the corotation radius? Are there some additional constraints to the Jacobi integral (cf. Fig. 1)?

To get a first insight into these questions, we have integrated several sets of orbits starting on 91 regularly spaced points on an elliptic arc aligned with the bar potential and joining $L_{1,2}$ to $L_{4,5}$:

$$\begin{array}{l} \{x_i, y_i, z_i\} = \{|x(L_{1,2})|\cos(\alpha_i), |y(L_{4,5})|\sin(\alpha_i), 0\}, \\ \alpha_i = i^\circ, \quad i = 0, 1, \ldots 90, \\ |x(L_{1,2})| = 6.27247, \quad |y(L_{4,5})| = 5.575744. \end{array} \tag{7}$$

The bar mass is chosen slightly larger ($G M_B = 0.63169379$) than the marginal $L_{4,5}$ stability value ($G\tilde{M}_{\rm B} = 0.62169379$). The total mass remains fixed to 1. The situation would correspond to a bar that has grown up to slightly overshoot the $L_{4,5}$ stability condition.

Here we show the initial velocities of orbits of the set starting with a modulus of ≈ 0.07 in the rotating frame, and various directions:

$$\begin{array}{rcl} \{\dot{x}, \dot{y}, \dot{z}\}(t=0) & = & \{0, 0, 0.07\}, \\ & & \{\pm 0.04, \pm 0.04, 0.04\}, \\ & & \{\pm 0.05, 0, 0.05\}, \quad \{0, \pm 0.05, 0.05\}. \end{array} \tag{8}$$

Other starting values have been used with similar results: faster initial conditions lead to larger diffusion, and vice-versa. A velocity of 0.07 matches conservatively a velocity dispersion of slightly less than $70\,{\rm km\,s^{-1}}$ at the corotation radius. For example, if the Galactic bar corotation lies at $R = 4\,{\rm kpc}$ and the velocity dispersion squared follows an exponential decrease with the same scale-length as the surface density one, then the expected velocity dispersion $R = 8\,{\rm kpc}$ for a disk scale-length of 4 kpc.

The orbits are integrated either up to 10 Gyr or when they first reach a radial distance of 50 kpc from the origin, which is the most frequent case. They are sampled at regular time intervals of 10 Myr.

The main result is that most of the trajectories diffuse fast, in one or two rotation periods beyond twice the corotation radius. The horizontal diffusion is clearly constrained inside corotation to a few "channels" for orbits starting near $L_{1,2}$ (Fig. 9, top).

As visible in Fig. 9, bottom, the envelope of diffusion in z beyond corotation is approximately linearly increasing with R: $z_{\rm max} \propto 0.1\,R$ to $0.25\,R$. The additional constraint well beyond corotation is the "third integral" (Contopoulos 1963)[5]. As visible when comparing the $\alpha \leq 10^\circ$ frame in Fig. 9, bottom, to the $\alpha \geq 45^\circ$ frames, the confinement due to an effective integral is stronger for orbits starting around $L_{1,2}$ than around $L_{4,5}$.

A few orbits diffuse differently, rather vertically at more than 2 kpc while above the bar. Fig. 9, bottom, shows clearly that the complex instability associated to $L_{4,5}$ and its associated chaotic phase-space structure allows stars to diffuse higher in z and also above the bar in the inner stellar halo, than the simple instability associated to $L_{1,2}$.

The average surface density of these diffusing, mostly chaotic looking orbits is asymptotically tending toward an exponentially decreasing radial distribution, as already described in P85b.

8. Discussion

A general statement can be made about the evolution of bars. In general as a bar grows, its strength increases until a critical value is reached beyond which the Lagrangian points are all fully unstable in the galaxy plane. While the instability around $L_{1,2}$ may concern a relatively modest fraction of the corotation circle, because the rest may be trapped by stable banana orbits circling around the stable $L_{4,5}$, this possibility disappears completely when the points $L_{4,5}$ become complex unstable. Phase space is then largely composed of unstable or chaotic orbits: a general orbital instability must be expected around the corotation circle, *including the amplification of the oscillations transverse to the galactic plane.*

When corotation is fully unstable, one expects a fast, mostly radial diffusion of its stars toward several times the corotation radius. But the z-amplitude increases almost

[5] This additional "integral" is only approximate. It comes from the flatteness of galactic disks: near the galaxy plane the z motion is nearly harmonic and, more important, almost decoupled of radial motion. Since any one-dimensional oscillator (harmonic or not) is integrable (see e.g., Lichtenberg & Lieberman 1992), phase space is close to have an additional integral of motion for low z amplitude, near circular orbits.

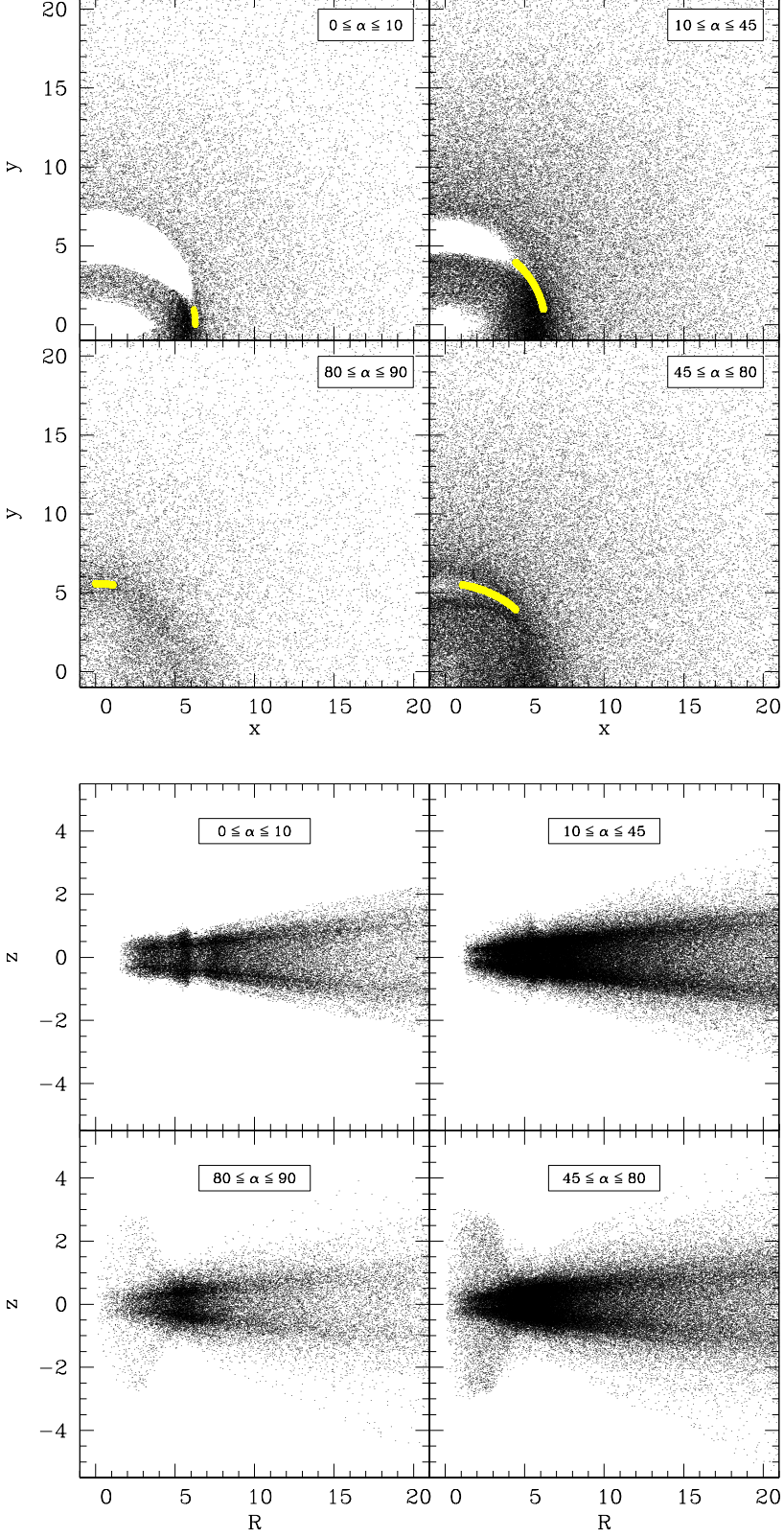

Fig. 9. Radial (top) and vertical (bottom) extensions of orbits sampled at regular time intervals and starting on the corotation ellipse (shown by light-gray areas in the top four frames), with various angles α from the x-axis. The initial velocities in the rotating frame are similar to the velocity dispersion in a barred galaxy at this radius. Clearly, orbits starting near the complex unstable $L_{4,5}$ can diffuse to more than 2 kpc above the bar region, while most of the orbits diffuse to large R and moderate $|z|$.

centre. This is clearly a new channel for lifting matter out of the galactic plane beside the vertical Inner Lindblad resonances able to feed a bulge as described in P84, Combes et al. (1990) and Pfenniger & Friedli (1991). The average orbital density of diffusing chaotic orbits outside corotation is exponentially decreasing in R, as shown in P85b. This is interesting because a stellar bar is a well known mechanism to produce the double exponential distribution observed in typical stellar disks (Hohl 1971; PF91; Courteau et al. 1996), the transition from the inner steep exponential to the outer shallower one being just fixed by the corotation radius.

In P90 we had shown that self-consistent N-body bars tend to reach the marginal stability state around $L_{4,5}$, as if the whole system self-regulates its degree of instability around corotation to a minimum. So the stability of the Lagrangian points seem to play a global role in barred galaxies.

Schematically, the evolution of barred galaxies can be described by the following stages. First, an axisymmetric disk becomes bar unstable for various reasons, such as a disk kinematical cooling by star formation (Carlberg & Sellwood 1984), or by a tidal interaction (Noguchi 1988, 1996). The bar growth becomes then rapidly non-linear and proceeds with a time-scale of order of the rotation period. When the bar becomes strong enough, the Lagrangian points $L_{4,5}$ reach the threshold of complex instability (P90) and matter around them is evacuated away, diffusing by about $1-5$ kpc around the galactic plane and several 10 kpc in the radial direction in a few rotational periods. This latter effect is suggested by observations: several barred galaxies do appear particularly dark in the region corresponding to the Lagrangian points $L_{4,5}$. Examples are NGC 3504, or NGC 4394 in the Hubble Atlas (Sandage 1961). These holes in the stellar distributions can only be repopulated by fast moving stars able to cross the corotation circle. Therefore the average stellar kinetic "temperature" must rise, moderating or even stopping the bar growth. Eventually a marginal stable state of the Lagrangian points $L_{4,5}$ follows.

As discussed previously (e.g., Pfenniger & Norman 1990; Hasan, Pfenniger & Norman 1993), secularly gas or infalling satellite accumulating within the ILR are able to dissolve completely the bar, which is another process determining the subsequent evolution of barred galaxies.

9. Conclusions

The 3D dynamical structure of phase space in barred galaxies around the Lagrangian points has been investigated. For parameters close to the ones suited to realistic barred galaxies the Lagrangian points L_4 and L_5 are not far from a marginal stability state. Beyond a critical bar strength these points become complex unstable, which means that ity is not restricted to a particular plane but is three-dimensional, though the approximate third-integral still constrains diffusion in z outside the corotation circle. Thus, stellar diffusion, and even for practical purpose escape, are particularly important in the radial direction.

Therefore stars in the corotation region can not only make wide excursions within the plane, but also substantial ones out of the plane. This important conclusion can be reached after the orbit analysis around $L_{4,5}$ because *the associated Hopf-like bifurcation is of inverse type*. Besides the already well-discussed vertical instabilities existing in bars, particularly the 2/1 vertical Inner Lindblad Resonance able to induce the formation of peanut-shaped bulges (e.g., Combes et al. 1990), this full instability provides an interesting channel for lifting matter into an extended thick disk made of stars born in the few inner kpc of a galaxy. Because this instability occurs at corotation, the diffusion of stars further out is much easier than in the case of the Inner Lindblad Resonance, because chaotic motion is no longer bounded by the zero-velocity surface linked to the Jacobi integral.

Several barred galaxies do appear to be particularly dark in the region corresponding to the Lagrangian points $L_{4,5}$. Besides the convenience to mark the location of corotation, these mass deficit regions suggest a secular evolution of these galaxies during which the strength of the bar increases up to the point that the Lagrangian point $L_{4,5}$ become complex-unstable, clearing for a while the region around them. Unless fully destabilized the system should react collectively by slowing down and even stopping the growth of the bar. In N-body experiments without dissipation (P90) it has been indeed found that the asymptotic state of pure stellar bars is to tend to keep the $L_{4,5}$ points marginally stable.

Acknowledgements. M. Ollé thanks P. Comas for his help in all computer and software issues, and is very grateful to the Geneva Observatory, where this work was done. We thank G. Contopoulos and D. Friedli for interesting comments on the manuscript. The first author has been partially supported by DGICYT grant no. PR95-240 and CIRIT grants no. 1995BEAI-400002 and GRQ93-1135. This work was also supported by the Swiss National Science Foundation (SNSF). The Povray team is acknowledged for its free ray-tracing software used for Fig. 3.

References

Binney J., Tremaine S. 1987, Galactic Dynamics, Princeton Univ. Press
Broucke R., 1969, AIAA J. 7, No 6, 1003
Carlberg R.G., Sellwood J. A. 1984, ApJ 282, 61
Combes F., Debbash F., Friedli D., Pfenniger D. 1990, A&A 233, 82
Contopoulos G. 1963, AJ 68, 1
Contopoulos G. 1981, A&A 102, 265
Contopoulos G. 1988, Cel. Mec. 43, 147

Contopoulos G., Magnenat P. 1985, Cel. Mech. 37, 387
Courteau S., De Jong R. S., Broeils A. H. 1996, ApJ 457, L73
Ferrers N.M. 1877, Quart. J. pure Appl. Math. 14, 1
Fux R. 1997, A&A, 327, 983
Hadjidemetriou J.D. 1975, Cel. Mech. 12, 255
Hasan H., Pfenniger D., Norman C. 1993, ApJ 409, 91
Heggie D.C. 1985, Cel. Mec. 35, 357
Hohl F. 1971, Astrophys. J. 168, 343
Kormendy J. 1982, in Morphology and Dynamics of Galaxies, 12th Saas Fee Lectures, (L. Martinet and M. Mayor eds.), Geneva Observatory, Geneva, 115
Lichtenberg A.J., Lieberman M.A. 1992, Regular and Chaotic Dynamics, Second edition, Springer-Verlag, New York
Magnenat P. 1982, Cel. Mech. 28, 319
Magnenat P. 1982, A&A 108, 89
Martinet L., Pfenniger D. 1987, A&A 173, 81 (MP87)
Miyamoto M., Nagai R. 1975, PASJ 27, 533
Nagai R., Miyamoto M. 1976, PASJ 28, 1
Noguchi M. 1988, A&A 203, 259
Noguchi M. 1996, AJ 469, 605
Pfenniger D. 1984, A&A 134, 373 (P84)
Pfenniger D. 1985a, A&A 150, 97 (P85a)
Pfenniger D. 1985b, A&A 150, 112 (P85b)
Pfenniger D. 1987, A&A 180, 79 (P87)
Pfenniger D. 1990, A&A 230, 55 (P90)
Pfenniger D. 1995, in Three-Dimensional Systems, IXth Florida Workshop in Nonlinear Astronomy, H.E. Kandrup, S.T. Gottesman, J.R. Ipser (eds.), Ann. New York Acad. Sci. 751, 131
Pfenniger D., Friedli D. 1991, A&A 270, 561
Pfenniger D., Norman C.A. 1990, ApJ 363, 391
Raha N., Sellwood J. A., James R. A., Kahn F. D. 1991, Nature 352, 411
Sandage A. 1961, The Hubble Atlas of Galaxies, Carnegie, Washington
Wakamatsu K.-I., Hamabe M. 1984, ApJS 56, 283
Zhao H. 1996, MNRAS 283, 149